Sulphide GaxGe25–xSb10S65(x=0,5) sputtered films: Fabrication and optical characterizations of planar and rib optical waveguides

Joël Charrier, Marie-Laure Anne, Hervé Lhermitte, J.-P. Guin, Virginie Nazabal, Frédéric Charpentier, Thierry Jouan, Frederic Henrio, Dominique Bosc, Jean-Luc Adam

Sulphide $Ga_xGe_{25-x}Sb_{10}S_{65(x=0,5)}$ sputtered films: Fabrication and optical characterizations of planar and rib optical waveguides

J. Charrier,[1] M. L. Anne,[2] H. Lhermite,[3] V. Nazabal,[2,a)] J. P. Guin,[4] F. Charpentier,[2] T. Jouan,[2] F. Henrio,[1] D. Bosc,[1] and J. L. Adam[2]
[1]*FOTON-CCLO, UMR 6082-ENSSAT, Université Rennes 1, 22305 Lannion, France*
[2]*Sciences Chimiques de Rennes, UMR-CNRS 6226, Equipe Verres et Céramiques, Université Rennes 1, 35042 Rennes, France*
[3]*IETR-Microelectronique, Université Rennes 1, 35042 Rennes, France*
[4]*LARMAUR, FRE-CNRS 2717, Université Rennes 1, 35042 Rennes, France*

(Received 16 April 2008; accepted 12 June 2008; published online 7 October 2008)

We report the fabrication and the physical and optical characterizations of sulphide $Ga_xGe_{25-x}Sb_{10}S_{65(x=0,5)}$ rib waveguides. High quality films fabricated on SiO_2/Si wafer substrates were obtained using the sputtering magnetron rf deposition method. The slab waveguides obtained without annealing present propagation losses of about 0.6 dB/cm at 1550 nm. These optical losses are not important for implementation in optical devices based on silicon-on-insulator or polymer, for instance, atomic force microscopy measurements revealed low interface roughness between the different media (substrate/film and film/air). Reactive ion etching was used to pattern rib waveguides between 2 and 300 μm wide. The parameters were optimized to obtain a dry etching process that had low surface roughness, vertical sidewalls, etch depth of more than 1 μm, and reasonable etching rate. This technique was used to fabricate *Y* optical junctions for optical interconnections on chalcogenide amorphous films. Their optical transmission was demonstrated by optical near field of guided modes and optical losses were measured and discussed. © *2008 American Institute of Physics*. [DOI: 10.1063/1.2968248]

I. INTRODUCTION

In the many fields where integrated optics can be used, the development of amplifiers and laser sources, optical sensors, and all-optical devices based on nonlinear properties will be able to provide low cost and highly compact optical systems. Chalcogenide glass offers advantages such as a wide transmission window (1–20 μm) depending on the material's compositions and its high refractive index, making integrated optics suitable for sensitive detection of biological or environmental variations.[1–6] They also present interesting nonlinear optical properties, photorefractive effects, and low phonon energies for active devices. These properties (wavelength conversion, Raman and parametric amplification, laser sources for mid-IR, etc.) are actually under investigation on fibers and planar waveguides made of chalcogenide glass.[7–18]

Slab waveguides based on chalcogenide amorphous films with good adherence and controlled composition may include rare earth ions. They can be obtained using different methods of deposition such as thermal evaporation,[19–22] chemical vapor deposition,[23] pulsed laser deposition,[24–27] and rf sputtering.[28–30] The first step was to produce rib waveguides, i.e., two-dimensional guiding structures composed of a thin high-index layer deposited on a low-index substrate. Lithography and plasma etching are standard patterning techniques in microelectronics used to design and manufacture complex optical devices on a compact chip.

The aim of this study is to obtain sulphide waveguides using rf-magnetron sputtering showing a low surface roughness and low optical losses. The composition of the films $Ge_{25}Sb_{10}S_{65}$ and $Ga_5Ge_{20}Sb_{10}S_{65}$ (called 2S1G and 2S2G, respectively) were also selected for their transparency in the visible and near-IR domain compared to selenide and telluride films, their glass transition temperature higher than 300 °C related to the network cross-linkage strengthened by the presence of fourfold coordinated germanium atoms and their faculty to accept rare earth doping in the case of 2S2G with partial substitution of gallium for germanium.[27,31–33]

II. EXPERIMENTAL CONDITIONS

A. Synthesis of targets, film deposition, and characterizations of the sputtered films

Chalcogenide glass targets were synthesized from commercial elemental precursors (Ga, Ge, Sb, and S) of high purity (5*N*). The precursors despite their high nominal purity often present a surface oxidation and can be polluted by water. So, sulfur was purified before the synthesis by dynamic and static distillation to remove impurities and then was kept in a glove box under dry argon atmosphere. All the elements were placed in evacuated quartz ampules and then sealed. The synthesis was performed in a rocking furnace at a temperature of 800 °C for 12 h. The ampule containing the melt was then air quenched. Targets were directly obtained from glass rods in the form of cylinders with 5 mm thickness and 50 mm in diameter.

a)Electronic mail: virginie.nazabal@univ-rennes1.fr.

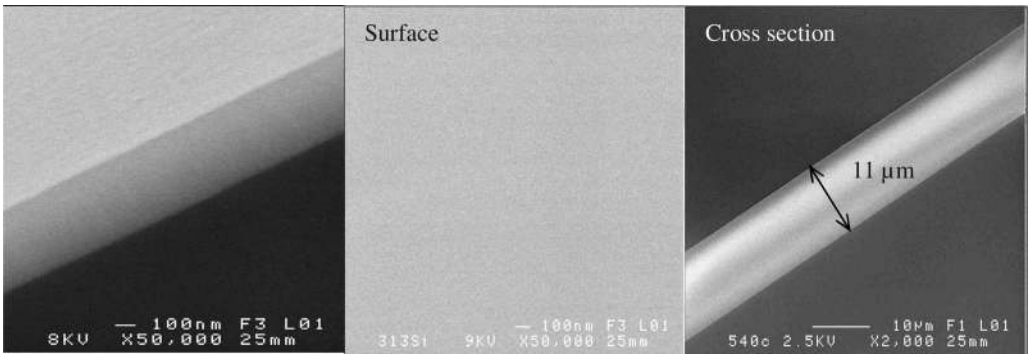

FIG. 1. SEM images of cross sections and surface of sulphide thin films deposited by rf-sputtering.

The starting substrates measured 1.5 in. Si wafers. They were wet oxidized at 1175 °C in an open tube furnace for 10 h. Oxide thickness was measured with a Taylor–Hobson profilometer and was equal to 2.7 μm.

2S2G and 2S1G films were deposited by rf-magnetron sputtering on top of these surface oxidized silicon substrates. Deposition was carried out at a working pressure in the range of 5.10^{-3}–5.10^{-2} mbar. The sputtering power was maintained at low rf power (15–50 W) during deposition.

The layer and rib waveguide surface and their roughnesses (rms) were analyzed both by field emission scanning electron microscopy (SEM) (JEOL JSM 6301F) and by atomic force microscopy (AFM) using tapping mode™ with 10 nm tip radius cantilevers (Nanoscope III, Digital Instruments).

B. Photolithography and dry etching methods

A classical photolithography process was used to prepare dry etching with positive Shipley S1813 photoresist. First, a 1.3 μm thick photoresist was spin coated on the wafers. After soft baking, the photoresist was then exposed to UV by means of a Cr-mask using a Suss Microtech MJB3 *i*-line mask aligner. The exposed bands were dissolved with a commercial developer. Considering the high reactivity of chalcogenide films in relation to the NH_4OH- or KOH-based developer, the TMAH-based developer Microposit MF 319 was selected. After hard baking, different parameters were investigated in the etch process: study of the gas composition (either CF_4 or CHF_3 and combined with O_2), gas flow from 1 to 30 SCCM (SCCM denotes cubic centimeter per minute at STP), gas pressure between 0.3 and 30 mTorr, and rf power in the range of 30–300 W. The etching was performed with a Nextral NE 110 reactive ion etching (RIE) machine to obtain both vertical and smooth sides. The CF_4 and CHF_3 gases were selected since the F^- ions could form volatile compounds with sulphide glass. The etch rates were determined by SEM observation of film cross sections.

C. Optical characterization

The effective refractive indices of the propagation modes in the planar waveguide were measured with a Metricon-2010 laser beam with wavelengths 633, 1302, and 1540 nm for both TE and TM polarization and rutile prism were used to excite the TE and TM modes inside the planar chalcogenide waveguides.

Optical losses were measured by studying the scattered light from the surface of the waveguides. These waveguides varied in length from 2 to 2.5 cm.[34,35] The laser light was single-mode fiber-coupled into the waveguide. The intensity of the scattered light was recorded with a digital camera placed above the sample. Transverse scanning along the direction of light propagation enabled us to obtain the two-dimensional (2D) light intensity distribution of the waveguide modes. The longitudinal variation was obtained by integrating the data along each sampling transverse line. The light intensity decreased exponentially with the

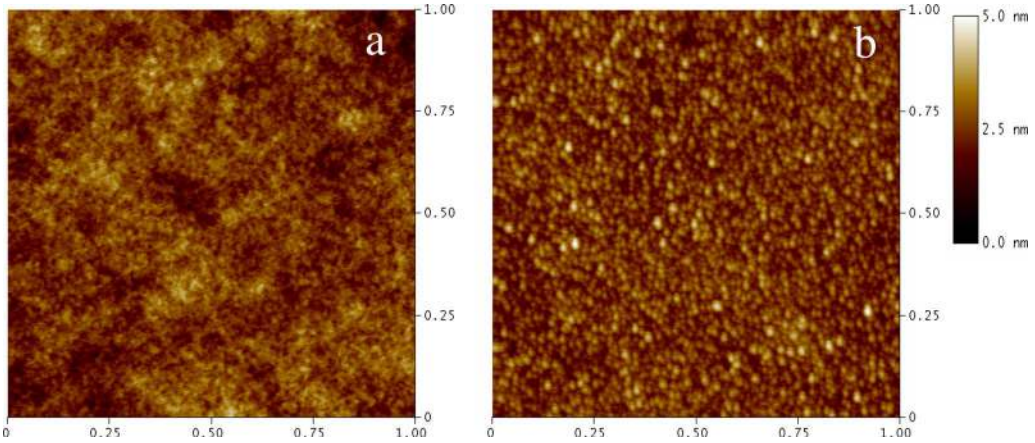

FIG. 2. (Color online) AFM image of a 1×1 μm^2 area of a 2S2G deposited film.(a) Film with thickness=2 μm and (b) film with thickness=6 μm.

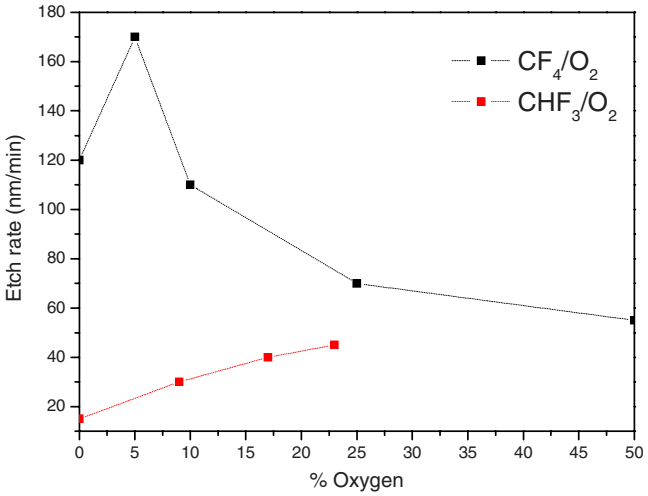

FIG. 3. (Color online) Etch rate of 2S2G films as functions of O_2/CF_4 gas flow ratios, with a plasma power 100 W, pressure 3 mTorr, and 10 SCCM CF_4 flow rate.

z-propagation distance. In this study, the attenuation values were the average of several measurements performed on several samples. The polarization of the coupled light in the waveguide was not controlled.

In addition, light propagation was observed at the output of the waveguides by recording near field profiles of guided modes at 1550 nm.

III. RESULTS AND DISCUSSION

A. Morphology and topography of the native and etched films

The 2S2G and 2S1G film deposition rate varied from 10 to 20 nm min^{-1} depending on the target composition and the distance between substrate and target. In these deposition conditions, the thickness of thin films varied from 0.5 to 20 μm.

SEM technique was applied to study the morphology of thin films, as shown in Fig. 1. Neither columnlike structure in the cross section nor cracks at the surface of the 11 μm thick films were observed. The layers seemed to be dense.

The rms roughness was determined by AFM, over a 1 $\times 1$ μm^2 area, before and after annealing for several different thicknesses (Fig. 2). The roughness slightly increased nonlinearly, the roughness being 0.2 nm for a film of about 2 μm in thickness, 0.25 nm for 4 μm, and 0.4 nm for 6 μm. After annealing near the glass transition temperature range, no changes in the roughness were observed. Similar results were obtained for both 2S2G and 2S1G films.

At this stage, the optical quality of films deposited by rf sputtering was sufficiently high to obtain rib waveguides by dry etching with fluorinated gases. The problem with chalcogenide films is to achieve vertical sidewalls that are not inwardly or outwardly tapered. So, we varied etching conditions in the capacitive plasma method and the gas used. For RIE using CF_4 plasma, the etching rate for 2S1G and 2S2G was typically about 300 and 100 nm min^{-1}, respectively (100 W, 3 mT, and 10 SCCM). A clear isotropic feature with lateral undercuts was observed for these etching parameters with a higher pressure (30 mT). However, a positive effect was that the etching rate rose by a factor of about 1.5. The CHF_3 gas was selected to minimize the undercutting of the sidewalls due to the formation of protective fluorocarbon polymer layer. However, the use of the CHF_3 gas was finally less efficient in terms of etch rate. The optimized conditions enabled etch rates of about 15 nm min^{-1} for 2S2G and 30 nm min^{-1} for 2S1G (100 W, 3 mT, and 25 SCCM) to be obtained. The lower etch rate in CHF_3 is certainly due to a greater thickness of the fluorocarbon film deposited on the chalcogenide film surface during steady-state etching. Indeed, it was demonstrated that etch rate is strongly influenced by the deposition of polymer film using CF_4 or CHF_3 gas.[36] The F/C ratio of CHF_3 smaller than that of the CF_4 gas was expected to decrease the etchant concentration of fluorine by forming HF and promoting the passivation of the sulphide film by polymerization. A compromise was looked for the effects of the addition of oxygen into the plasma. In these conditions of these etching parameters, CHF_3/O_2 plasma containing 30% of oxygen provided a better etch rate that was three times higher than the previous one but was still slow. For CHF_3 plasma, sidewalls with overcut angles lower than 20° were obtained by controlling the etching pa-

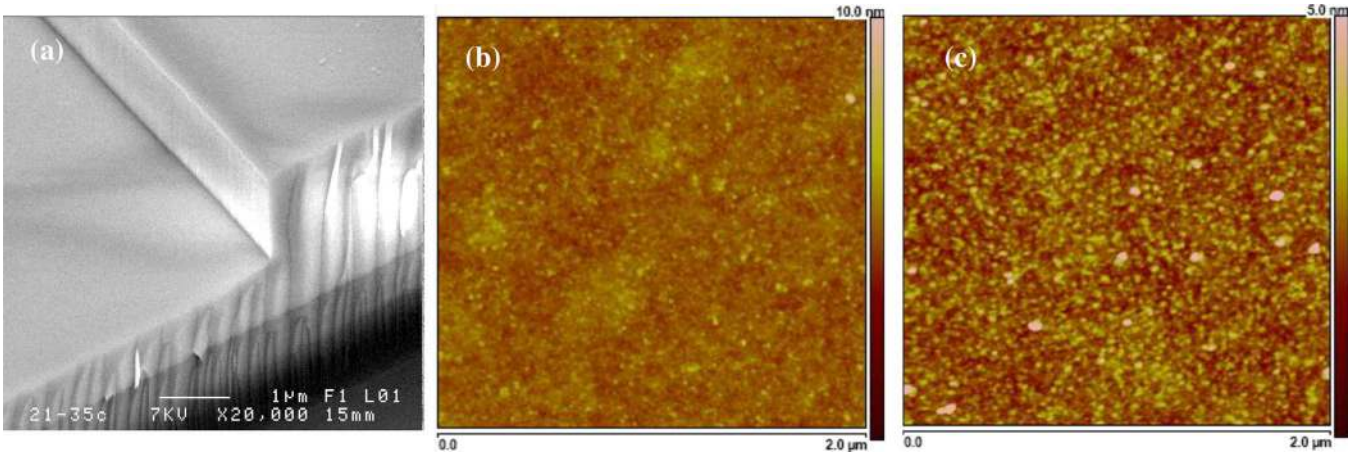

FIG. 4. (Color online) SEM images showing rib waveguide made of 2S1G deposited by sputtering and AFM image of a 2×2 μm^2 area of a 2S1G deposited film.(a) Etched surface area, (b) surface of the rib waveguide before etching, and (c) surface of the rib waveguide after etching.

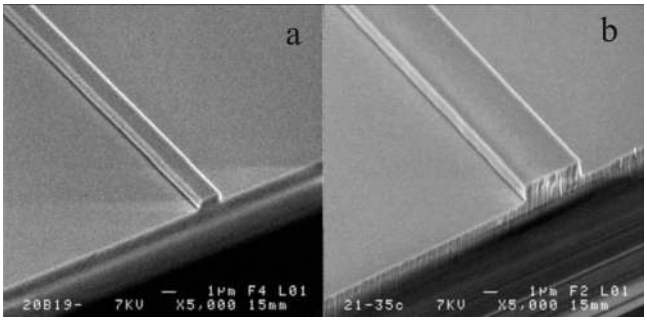

FIG. 5. SEM images showing rib waveguide made of 2S2G and 2S1G deposited by sputtering.

rameters. The addition of oxygen to CF_4 plasma during the etching of 2S2G or 2S1G films was also explored but it did not considerably enhance the etch rate and as the proportion of oxygen increased, the etch rate decreased. Figure 3 illustrates the dependencies of etch rate on the O_2/CF_4 gas flow ratios when the power was 100 W and the pressure was maintained at 3 mT. The O_2/CF_4 plasma etch rate of 2S2G increased to 180 nm min^{-1} before dropping to 60 nm min^{-1} when the plasma had over 50% of oxygen. The initial increase could be related to the dissociation of CF*x* radicals in the plasma, due to the production of carbon oxides.[37] Then, the concentration of reactive fluoride compounds in the plasma decreased due to dilution by oxygen and the possible formation of oxides or an oxysulphide layer.

Due to these low etching rates obtained of CHF_3 gas for the parameters under considerations even with O_2/CHF_3 gas mixture, we turned our attention to CF_4 gas in order to obtain an anisotropic etching of the sulphide films with suitable etch rate. Finally, the dry etching process used allowed a good etching selectivity, uniformity, satisfactory etching rate, and straight sidewalls (Figs. 1 and 4). Thus, some rib waveguides were fabricated with width from 2 to 400 μm and etch depth from 0 to 3 μm avoiding an excessive etching at the sidewalls leading to undesirable sloped sidewalls. The roughness evolution of the film after photolithography and CF_4 etching was controlled by SEM and AFM at the end of the process after the removal of the photoresist from the waveguide. These two techniques analyzed both the surface of the sulphide waveguide protected during the etching by the photoresist and the one etched (Figs. 4 and 5). After photolithography, dry etching, and photoresist stripping, the roughness of the 2S1G film of about 1.5 μm thick is about 0.25 nm both on the etched surface and on the top of the rib waveguide (Fig. 4). The surface roughness slightly increases in the case of 2S2G compared to 2S1G due to insufficient removal of gallium during the etching process, as expected for such chemical element with fluorine gas. This effect can be compensated by increasing the rf power associated with a low pressure (Fig. 5).

TABLE I. Characteristics of guiding and cladding layers. The refractive index was measured at 1550 nm using *m*-lines method.

Type of material	Refractive index at 1550 nm	Thickness layer (μm)
2S1G glass	2.238	1.7
2S2G glass	2.245	1.2
SiO_2	1.447	2.7

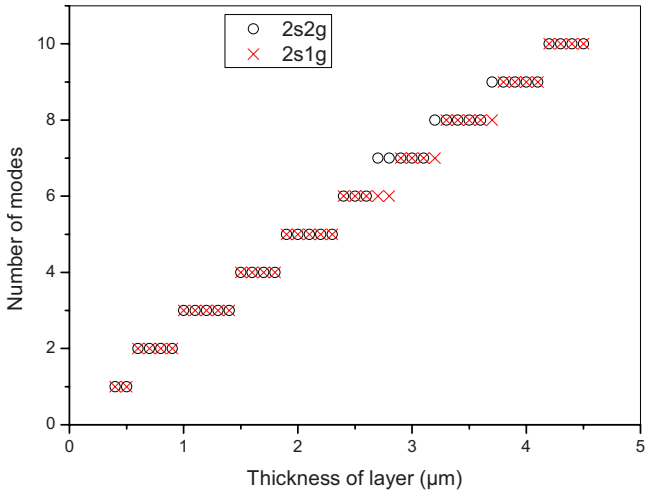

FIG. 6. (Color online) Calculated number of modes as a function of the thickness of guiding layer for a 2S1G and 2S2G slabs waveguides at 1550 nm.

B. Modal characterization

The refractive indices were measured by *m*-lines method at 1550 nm. These measurements are shown in Table I. From these results, the propagated modes were calculated using the dispersion equation for a slab waveguide as a function of the thickness of the guiding layer (Fig. 6). The effective refractive index values of the first modes are presented in Table II. Each of the guided modes propagates by total internal reflection with an angle θ with respect to the perpendicular at the interface guiding layer/cladding layer. The values of these angle and their effective thickness are also shown in Table II.

In order to check the modal character of waveguide, the guided modes were observed at the output of the waveguides using a near field method at 1550 nm for slab and rib waveguides [Figs. 7(a) and 7(b)]. These measurements reveal that these waveguides are multimode for both slab (according to vertical direction) and rib structures.

C. Optical loss measurements

Optical losses were measured for the different types of waveguides. The measured attenuation coefficient mainly depended on: material absorption (α_{abs}), surface scattering (α_{surf}), interface roughness and volume scattering (α_{vol}), and the inhomogeneity of the refractive index and radiative losses (α_{rad}). Thus, the overall attenuation was equal to the sum of all these optical loss contributions. The measured values are shown in Table III at 1550 nm. In the case of the slab waveguides, the optical losses were always lower when using 2S1G waveguides than those obtained using 2S2G waveguides. This behavior could be explained by the presence of gallium in the 2S2G film for which a Raman scattering characterization revealed the possible formation of sulphide gallium clusters inside the glass that were not perfectly well dispersed inside the glassy matrix even for sulfur rich

TABLE II. Modal characteristics of slab waveguides at 1550 nm for TE polarization.

Type of slab waveguide	Mode number (at 1550 nm)	Effective index	θ (radians)	Effective thickness (μm)
2S1G	$m=0$	2.226	1.50	4.77
	$m=9$	1.553	0.77	5.15
2S2G	$m=0$	2.239	1.50	4.77
	$m=9$	1.570	0.78	5.11

glass.[38] In the case of the 2S1G rib waveguides, using the lowest widths (4 to 10 μm), the loss values were nearly constant and are around 0.9 ± 0.3 dB/cm whereas losses were reduced with the highest widths. These loss values were equal to those obtained on slab waveguides. For rib waveguides, we took into consideration not only the same loss origins, but also the presence of a few defects due to the photolithography process and the presence of edges. The overlap between guided modes and interface increased therefore the participation of surface scattering became more important. This could explain the difference of losses between planar and rib waveguides using small widths. This loss difference was estimated to be about 0.3 dB/cm.

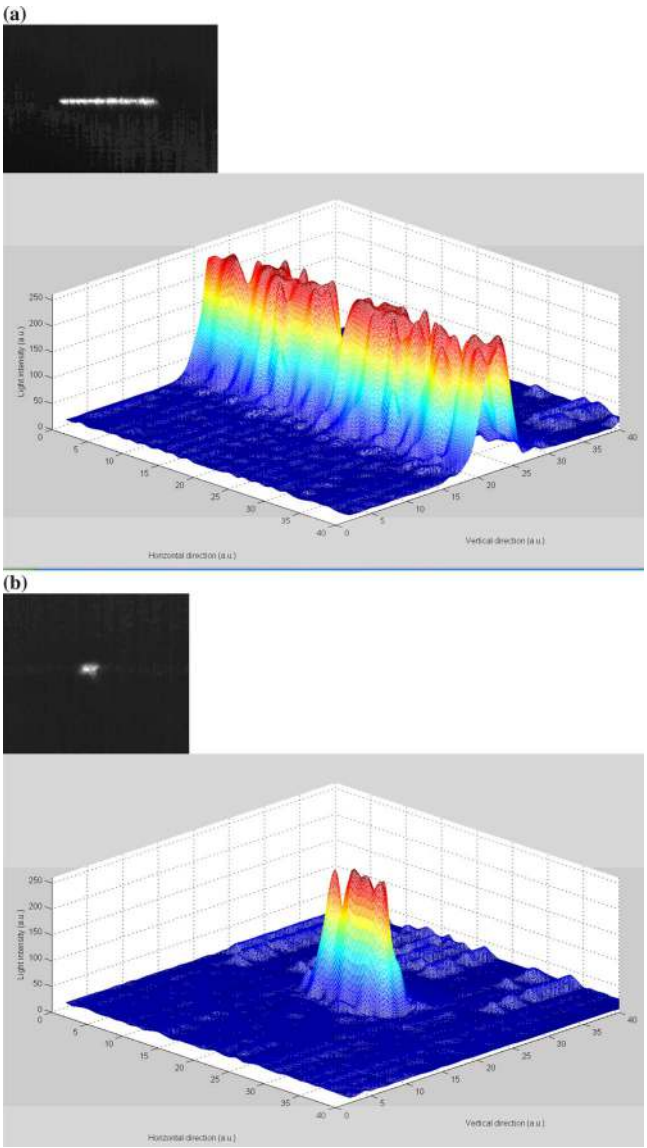

FIG. 7. (Color online) (a) Near field of guided modes for a 2S1G slab waveguide at 1550 nm and (b) near field of guided modes for a 2S1G rib waveguide with an 8 μm width at 1550 nm.

D. Theoretical optical losses

Four reasons have already been invoked to explain the origin of optical losses: (i) absorption, (ii) volume scattering, (iii) surface scattering, and (iv) radiative modes. In order to discuss the experimental results, the different factors of losses were calculated in order to establish the principal trends of different contributions.

(i) (ii) The value of losses due to absorption and scattering volume was estimated using the attenuation optical losses obtained for an optical fiber manufactured with the same material.[39] In this study, the 2S2G and 2S1G films are homogeneous and dense (SEM and AFM analysis). So, the refractive index was considered as constant in depth. As a result, the volume scattering losses can possibly be neglected in first approximation. At 1550 nm, the absorption coefficient was majored and was equal to 7×10^{-3} cm^{-1} corresponding to 3×10^{-2} dB/cm. This value was low enough to conclude that absorption by the material did not significantly contribute to losses.

(iii) In order to evaluate the lineic losses due to substrate leaky modes, these losses were calculated by using transfer matrix formalism,[40] considering a slab waveguide of homogeneous permittivity $\varepsilon_g=n_{2S1G}^2$, of thickness $t=4.5$ μm, between the air ($\varepsilon_A=1$), and a homogeneous cladding layer of permittivity $\varepsilon_c=n_{SiO_2}^2$, deposited on silicon substrate. In geometric optics, each of the guided modes propagates by total internal reflection, with an angle $\theta_{(n)}$ with respect to the main z-axis. Here we would find approximately $\theta_{(0)}\approx4.2°$ and $\theta_{(9)}\approx45.3°$ for the first and last modes. Over a projected length $\Delta z_{(n)}=2t\ \mathrm{cotan}(\theta_{(n)})$, the ray experiences two total reflections, one at each boundary. One can suppose that one of them is replaced by a reflectivity coefficient $R_{(n)}=1-L_{(n)}$ obtained from transfer matrix formalism. Then, by equating the latter with $\exp[-a_{(n)}\Delta z_{(n)}]\approx1-a_{(n)}\Delta z_{(n)}$, one can define an equivalent loss coefficient of $\alpha_{(n)}=L_{(n)}/\Delta z_{(n)}$. As a result, $\alpha_{(0)}$ is equal to 10^{-12} m^{-1} ($\approx8\ 10^{-14}$ dB/cm) and $\alpha_{(9)}\approx3\ 10^{-2}$ m^{-1} ($\approx1\ 10^{-3}$ dB/cm). So, in this study, the losses due to substrate leaky modes are considered negligible.

(iv) Surface scattering losses are related to the rms deviation of the planarity at guiding layer interfaces (σ).

TABLE III. Optical losses of 2S1G and 2S2G slab waveguides and 2S1G rib waveguide for different widths (w) at 1550 nm.

Optical losses (dB/cm)	2S2G slab waveguide	2S1G slab waveguide	2S1G rib waveguides	
			$15 \leq w(\mu m) \leq 300$	$10 \leq w(\mu m) \leq 3$
At 1550 nm	0.7 ± 0.3	0.6 ± 0.3	0.6 ± 0.3	0.9 ± 0.3

Light intensity lost by surface scattering at the two interfaces of the guiding layer is given by the model developed by Tien.[41] In this model, it is assumed that the roughness σ_{12} is constant at the (1) interface guiding layer and (2) cladding layer and is equal to 0.2 nm. (This roughness was measured by AFM). The roughness σ_{01} at the (0) interface air and (1) guiding layer is the parameter in this study. Figure 8 represents surface losses using a 2S1G slab waveguide at 1550 nm calculated as a function of roughness σ_{01} for the five first modes. The surface losses increase importantly with both the value of σ_{01} and with the mode order. The loss values can become very important as a function of the value of the roughness and could be the major source of losses.

E. Key results and realization of *Y* junctions

The difficulties inherent in the manufacturing of thick films and micron and nanosize structures in chalcogenide compared to oxide glass or silicon-on-insulator are well-known.[42–44] The choice of germanium based sulphide glass was fixed because of a better robustness expected with the presence of germanium atoms in the glassy network and a Tg relatively high for chalcogenide glasses.

The physical properties of these sulphide films turned out to be suitable for RIE etching. By optimizing the parameters for the pure CF_4 plasma process (power, gas pressure, and gas flow rate), an anisotropic etching behavior was obtained with a reasonable etching rate equal to 100 and 300 nm min^{-1}, respectively, for 2S2G and 2S1G and with an overcut angle (positively sloped sidewall) inferior to 10°. The O_2 gas mixed with fluorine gas was used, as observed in the case of $Ge_{33}As_{12}Se_{55}$ films, in order to increase the etching rate and yield overcut angles lower than 30°.[5,45] It was also used to limit, for pure CF_4 , the too strong chemical etch of As_2S_3 films leading to serious undercutting and very rough sidewalls of the waveguides.[46] The use of oxygen can be avoided in our case and allowed a better respect for the composition of the sulphide film limiting the formation of oxysulphide by oxygen diffusion into the film.

A single-mode fiber was used to couple light in the waveguides and the external field excited different modes. Although the simulation showed that these rib waveguides supported multiple modes at 1550 nm, higher order modes generally presented high losses due to the stronger coupling of the propagating field in relation to the sidewalls. As a result, the measured loss values include losses of several modes notably the surface scattering losses at different excited modes. The values of 0.6 dB/cm would be principally due to the contribution of surface scattering at different excited modes. Similar loss values of the same order of magnitude were obtained using multimode chalcogenide glass rib optical waveguides.[43,44]

Waveguide splitter are important elements in a variety of applications such as power splitters for planar lightwave circuits or optical sources for integrated microfluidic devices.[47] Such applications rely on the division of an optical signal into N outputs $(1 \times N)$. Finally, straight Y junctions with a guide width of 2 μm were formed on sulphide films by similar processes. Figures 9 and 10 show different top views of the structure and the near field, respectively, of guided modes at the output of the Y junction at 1550 nm. This struc-

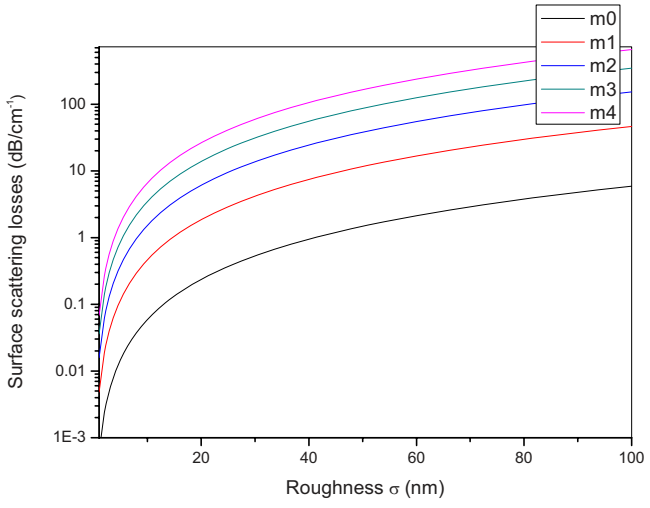

FIG. 8. (Color online) Surface scattering losses as a function of the roughness at the interface air/guiding layer for a chalcogenide glass slab waveguide at 1550 nm for different modes. The roughness is equal to 0.2 nm at the guiding layer/cladding layer.

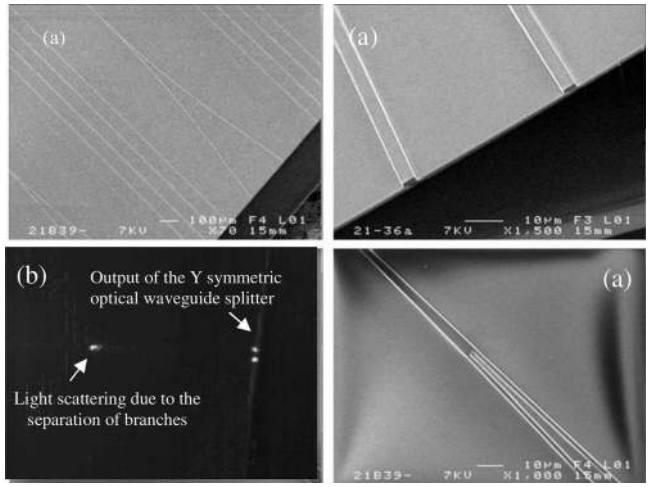

FIG. 9. (a) SEM micrographs showing Y junction rib waveguide made of 2S1G deposited by sputtering. (b) Top view of light guided in the symmetric beam splitter at 1550 nm.

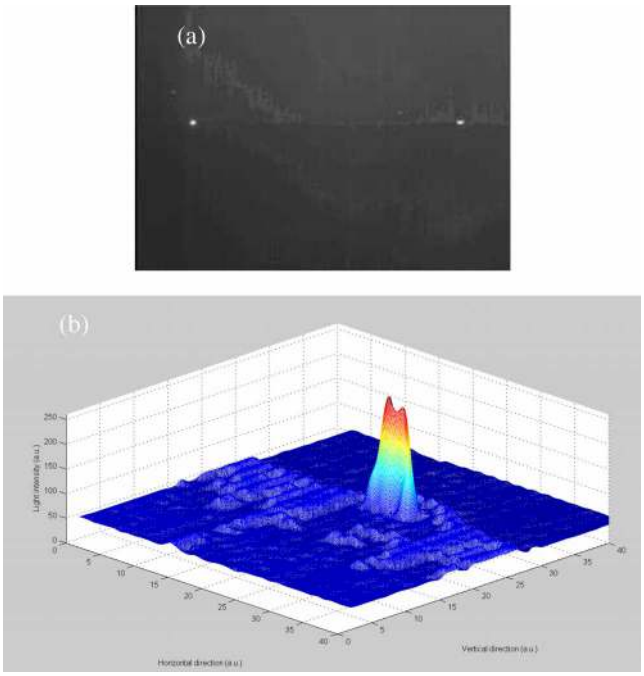

FIG. 10. (Color online) Near-fields of guided modes at the output of the *Y* symmetric optical waveguide splitter at 1550 nm (a) at 2D and (b) at three-dimension.

ture was designed in order to be slightly multimode with a film thickness of 500 nm and 4 μm width at the input and 2 μm after the *Y* junction. The top view (Fig. 9) of light transmission shows not only the scattering light at the outputs of the *Y* junction but also the scattering light due to the separation of branches. If an excess loss is expected for such structures it has not been possible to evaluate this yet.

IV. CONCLUSION

We have demonstrated the feasibility of manufacturing chalcogenide rib waveguides and *Y* junctions. Dry etching processes leading to low surface roughness, lower damage, reduced deviation from verticality of sidewalls, and reasonable etching rate were demonstrated. Optical losses as low as 0.6 dB/cm were measured at 1550 nm in slab and rib waveguides. The losses were principally due to surface scattering losses of different guided modes. The results suggest that germanium based sulphide amorphous films obtained by magnetron rf sputtering deposition method are suitable candidates for waveguide technology. This technology using the specific characteristics of chalcogenide glass has an excellent potential for application in different fields such as optical communication and sensing.

ACKNOWLEDGEMENT

The authors would like to thank P. Camy at CIMAP, UMR 6637 CEA-CNRS-ENSICaen, Université de Caen for advising us on waveguide patterning.

[1]M. L. Anne, V. Nazabal, V. Moizan, C. Boussard-Pledel, B. Bureau, J. L. Adam, P. Nemec, M. Frumar, A. Moreac, H. Lhermite, P. Camy, J. L. Doualan, J. P. Guin, J. Le Person, F. Colas, C. Compere, M. Lehaitre, F. Henrio, D. Bosc, J. Charrier, A.-M. Jurdyc, and B. Jacquier, Proc. SPIE **6475**, 647508 (2007).
[2]X. H. Zhang, G. Fonteneau, and J. Lucas, Vide, Couches Minces **44**, 99 (1989).
[3]J. Hu, V. Tarasov, A. Agarwal, L. Kimerling, N. Carlie, L. Petit, and K. Richardson, Opt. Express **15**, 2307 (2007).
[4]C. X. Yu, A. Ganjoo, H. Jain, C. G. Pantano, and J. Irudayaraj, Anal. Chem. **78**, 2500 (2006).
[5]V. Balan, C. Vigreux, A. Pradel, A. Llobera, C. Dominguez, M. I. Alonso, and M. Garriga, J. Non-Cryst. Solids **326-327**, 455 (2003).
[6]C. Vigreux-Bercovici, E. Bonhomme, A. Pradel, J. E. Broquin, L. Labadie, and P. Kern, Appl. Phys. Lett. **90**, 011110 (2007).
[7]T. Schweizer, D. W. Hewak, B. N. Samson, and D. N. Payne, J. Lumin. **72–74**, 419 (1997).
[8]M. Asobe, H. Itoh, T. Miyazawa, and T. O. N. Kanamori, Electron. Lett. **29**, 1966 (1993).
[9]G. Boudebs, F. Sanchez, J. Troles, and F. Smektala, Opt. Commun. **199**, 425 (2001).
[10]M. Guignard, V. Nazabal, F. Smektala, H. Zeghlache, A. Kudlinski, Y. Quiquempois, and G. Martinelli, Opt. Express **14**, 1524 (2006).
[11]P. Houizot, F. Smektala, V. Couderc, J. Troles, and L. Grossard, Opt. Mater. (Amsterdam, Neth.) **29**, 651 (2007).
[12]A. Saliminia, A. Villeneuve, T. V. Galstyan, S. LaRochelle, and K. Richardson, J. Lightwave Technol. **17**, 837 (1999).
[13]T. Cardinal, K. A. Richardson, H. Shim, A. Schulte, R. Beatty, K. Le Foulgoc, C. Meneghini, J. F. Viens, and A. Villeneuve, J. Non-Cryst. Solids **256-257**, 353 (1999).
[14]Y. Quiquempois, A. Villeneuve, D. Dam, K. Turcotte, J. Maier, G. Stegeman, and S. Lacroix, Electron. Lett. **36**, 733 (2000).
[15]V. G. Ta'eed, M. Shokooh-Saremi, L. B. Fu, D. J. Moss, M. Rochette, I. C. M. Littler, B. J. Eggleton, Y. L. Ruan, and B. Luther-Davies, Opt. Lett. **30**, 2900 (2005).
[16]A. K. Mairaj, A. M. Chardon, D. P. Shepherd, and D. W. Hewak, IEEE J. Sel. Top. Quantum Electron. **8**, 1381 (2002).
[17]C. Meneghini, J. E. Viens, A. Villeneuve, E. J. Knystautas, M. A. Duguay, and K. A. Richardson, J. Opt. Soc. Am. B **15**, 1305 (1998).
[18]A. K. Mairaj, C. Riziotis, A. M. Chardon, P. G. R. Smith, D. P. Shepherd, and D. W. Hewak, Appl. Phys. Lett. **81**, 3708 (2002).
[19]E. Marquez, T. Wagner, J. M. Gonzalez-Leal, A. M. Bernal-Oliva, R. Prieto-Alcon, R. Jimenez-Garay, and P. J. S. Ewen, J. Non-Cryst. Solids **274**, 62 (2000).
[20]J. Fick, E. J. Knystautus, A. Villeneuve, F. Schiettekatte, S. Roorda, and K. A. Richardson, J. Non-Cryst. Solids **272**, 200 (2000).
[21]S. A. Fayek and S. M. El-Sayed, NDT Int. **39**, 39 (2006).
[22]Z. G. Ivanova, K. Koughia, D. Tonchev, J. C. Pivin, and S. O. Kasap, J. Optoelectron. Adv. Mater. **7**, 1271 (2005).
[23]C. C. Huang and D. W. Hewak, Electron. Lett. **40**, 863 (2004).
[24]M. Frumar, B. Frumarova, P. Nemec, T. Wagner, J. Jedelsky, and M. Hrdlicka, J. Non-Cryst. Solids **352**, 544 (2006).
[25]K. E. Youden, T. Grevatt, R. W. Eason, H. N. Rutt, R. S. Deol, and G. Wylangowski, Appl. Phys. Lett. **63**, 1601 (1993).
[26]A. Zakery, Y. Ruan, A. V. Rode, M. Samoc, and B. Luther-Davies, J. Opt. Soc. Am. B **20**, 1844 (2003).
[27]V. Nazabal, P. Nemec, J. Jedelsky, C. Duverger, J. Le Person, J. L. Adam, and M. Frumar, Opt. Mater. (Amsterdam, Neth.) **29**, 273 (2006).
[28]D. A. Turnbull, J. S. Sanghera, V. Nguyen, and I. D. Aggarwal, Mater. Lett. **58**, 51 (2004).
[29]J. A. Frantz, J. S. Sanghera, L. B. Shaw, G. Villalobos, I. D. Aggarwal, and D. W. Hewak, Mater. Lett. **60**, 1350 (2006).
[30]S. Ramachandran and S. G. Bishop, IEEE J. Sel. Top. Quantum Electron. **11**, 260 (2005).
[31]Y. Guimond, J.-L. Adam, A.-M. Jurdyc, H. L. Ma, J. Mugnier, and B. Jacquier, J. Non-Cryst. Solids **256–257**, 378 (1999).
[32]V. G. Truong, A. M. Jurdyc, B. Jacquier, B. S. Ham, A. Q. Le Quang, J. Leperson, V. Nazabal, and J. L. Adam, J. Opt. Soc. Am. B **23**, 2588 (2006).
[33]V. Moizan, V. Nazabal, J. Troles, P. Houizot, J.-L. Adam, F. Smektala, G. Gadret, S. Pitois, J.-L. Doualan, R. Moncorgé, and G. Canat, Opt. Mater. (Amsterdam, Neth.) **31**, 39 (2008).
[34]Y. Okamura, S. Sato, and S. Yamamoto, Appl. Opt. **24**, 57 (1985).
[35]Y. Okamura, S. Yoshinaka, and S. Yamamoto, Appl. Opt. **22**, 3892 (1983).
[36]G. S. Oehrlein, Y. Zhang, D. Vender, and O. Joubert, J. Vac. Sci. Technol. A **12**, 333 (1994).
[37]W. T. Li, Y. L. Ruan, B. Luther-Davies, A. Rode, and R. Boswell, J. Vac. Sci. Technol. A **23**, 1626 (2005).
[38]M. Guignard, V. Nazabal, F. Smektala, J. L. Adam, O. Bohnke, C. Du-

verger, A. Moreac, H. Zeghlache, A. Kudlinski, G. Martinelli, and Y. Quiquempois, Adv. Funct. Mater. **17**, 3284 (2007).
[39]J. Troles, Y. Niu, C. Duverger-Arfuso, F. Smektala, L. Brilland, V. Nazabal, V. Moizan, F. Desevedavy, and P. Houizot, Mater. Res. Bull. **43**, 976 (2008).
[40]P. Pirasteh, J. Charrier, Y. Dumeige, S. Haesaert, and P. Joubert, J. Appl. Phys. **101**, 083110 (2007).
[41]P. K. Tien, Appl. Opt. **10**, 2395 (1971).
[42]D. Freeman, S. Madden, and B. Luther-Davies, Opt. Express **13**, 3079 (2005).
[43]Y. L. Ruan, W. T. Li, R. Jarvis, N. Madsen, A. Rode, and B. Luther-Davies, Opt. Express **12**, 5140 (2004).
[44]D.-Y. Choi, S. Madden, A. Rode, R. Wang, and B. Luther-Davies, Appl. Phys. Lett. **91**, 011115 (2007).
[45]M. W. Lee, C. Grillet, C. L. C. Smith, D. J. Moss, B. J. Eggleton, D. Freeman, B. Luther-Davies, S. Madden, A. Rode, Y. L. Ruan, and Y. H. Lee, Opt. Express **15**, 1277 (2007).
[46]N. J. Baker, H. W. Lee, I. C. M. Littler, C. M. de Sterke, B. J. Eggleton, D. Y. Choi, S. Madden, and B. Luther-Davies, Opt. Express **14**, 9451 (2006).
[47]Y. Qian, J. Song, S. Kim, W. Hu, and G. P. Nordin, Opt. Express **16**, 4981 (2008).